FEBS Letters

FEBS PRESS
science publishing by scientists

Crystal structure of archaeal HMG-CoA reductase: insights into structural changes of the C-terminal helix of the class-I enzyme

Bastian Vögeli[1], Seigo Shima[2], Tobias J. Erb[1] and Tristan Wagner[2,†]

1 Department of Biochemistry and Synthetic Metabolism, Max Planck Institute for Terrestrial Microbiology, Marburg, Germany
2 Microbial Protein Structure Group, Max Planck Institute for Terrestrial Microbiology, Marburg, Germany

Correspondence
T. Wagner, Microbial Protein Structure Group, Max Planck Institute for Terrestrial Microbiology, 35043 Marburg, Germany
Tel: +49 6421 178110
E-mail: twagner@mpi-bremen.de
T. J. Erb, Department of Biochemistry and Synthetic Metabolism, Max Planck Institute for Terrestrial Microbiology, Karl-von-Frisch-Straße 10, 35043 Marburg, Germany
Tel: +49 6421 178700
E-mail: toerb@mpi-marburg.mpg.de

[†]Present address
Microbial Metabolism Group, Max-Planck-Institute for Marine Microbiology, Celsius−Straße 1, 28359, Bremen, Germany

(Received 6 October 2018, revised 4 January 2019, accepted 22 January 2019, available online 22 February 2019)

doi:10.1002/1873-3468.13331

Edited by Stuart Ferguson

3-hydroxy-3-methylglutaryl-CoA reductase (HMGR) catalyses the last step in mevalonate biosynthesis. HMGR is the target of statin inhibitors that regulate cholesterol concentration in human blood. Here, we report the properties and structures of HMGR from an archaeon *Methanothermococcus thermolithotrophicus* (mHMGR). The structures of the apoenzyme and the NADPH complex are highly similar to those of human HMGR. A notable exception is C-terminal helix (Lα10-11) that is straight in both mHMGR structures. This helix is kinked and closes the active site in the human enzyme ternary complex, pointing to a substrate-induced structural rearrangement of C-terminal in class-I HMGRs during the catalytic cycle.

Keywords: cholesterol biosynthesis; isoprenoids; mevalonate biosynthesis; statins; structural rearrangement; X-ray crystallography

Mevalonate is the building block of isoprenoids and is formed through the mevalonate pathway [1]. This pathway involves the condensation of three molecules of acetyl-CoA to form 3-hydroxy-3-methylglutaryl-CoA (HMG-CoA). HMG-CoA is then reduced by the HMG-CoA reductase (HMGR) to generate mevalonate using four electrons from two molecules of NAD(P)H (Fig. 1A) [2]. Because HMGRs are the targets of statins, which are potent inhibitors that regulate human blood cholesterol levels [3], the catalytic mechanism of the eukaryotic and bacterial HMGR have been well-studied biochemically and structurally [4,5]. In archaea, HMGR is involved in the biosynthesis of membrane lipids. Despite this essential function of HMGR in archaea, studies on the enzyme are scarce, and no structures of archaeal HMGR have been reported thus far.

There are two classes of HMGR [5,6]. Class-I HMGRs are found in eukarya and archaea. They have a homotetrameric (dimer of homodimers) assembly and use

Abbreviations
CoA, coenzyme A; HMG-CoA, 3-hydroxy-3-methylglutaryl-CoA; HMGR, HMG-CoA reductase; mHMGR, HMGR from *Methanothermococcus thermolithotrophicus*.

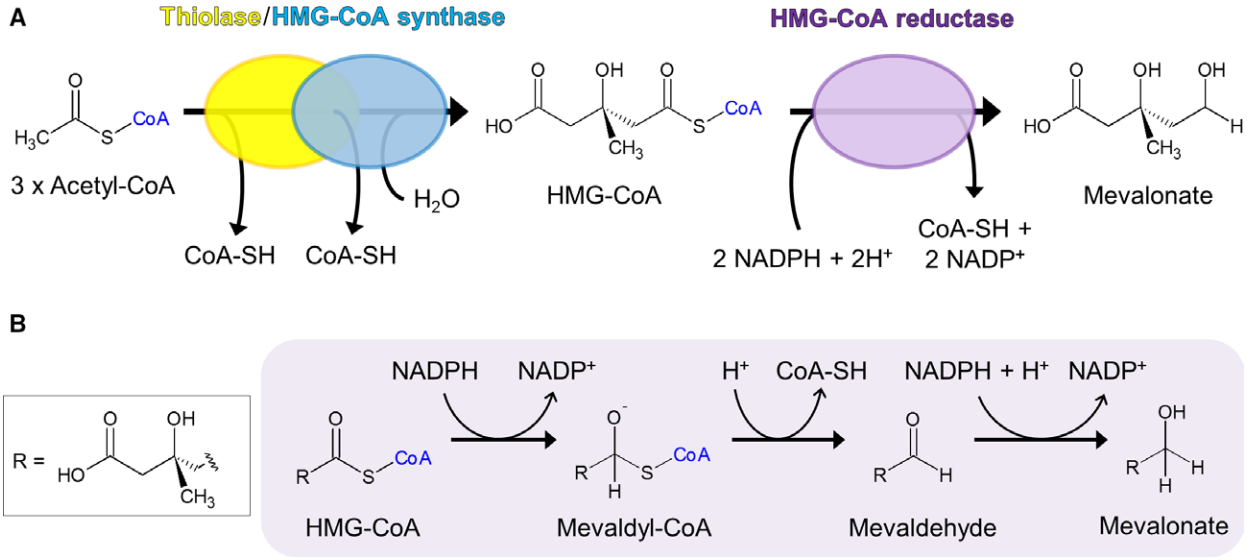

Fig. 1. Catalytic reactions in the mevalonate pathway and the HMGR-catalysed reactions. (A) Scheme of mevalonate production in methanogens starting from three acetyl-CoA molecules. The conversion of three molecules of acetyl-CoA to HMG-CoA is catalysed by an enzyme complex composed of thiolase and HMG-CoA synthase in archaea [18]. (B) The catalytic reactions of HMGR.

NADPH as a reductant. The eukaryotic class-I enzymes are composed of an N-terminal hydrophobic domain, a linker domain and a catalytic domain [6]. The hydrophobic domain functions as membrane anchor and has a regulatory function [7]. Archaeal and some eukaryotic class-I HMGRs do not have an N-terminal membrane anchor domain and only comprise of the catalytic domain [6]. As observed in the human HMGR, the catalytic domain forms the homodimeric assembly. The catalytic domain can be further subdivided to the N-terminal, large and small domains. The *cis*-loop links the small and large domains and contains the residues critical for HMG-CoA binding. Class-II HMGRs are found in bacteria and some archaea [6,8]. They form catalytic homodimers and have varying cofactor preference for either NADH or NADPH or both [9]. Class-I and class-II HMGRs share a catalytic domain core structure although the assembly of the small domain is different, and the class-II enzymes lack the *cis*-loop. Therefore, the arrangements of the active site differ in class-I and -II HMGRs [6].

The HMGR-catalysed reactions are shown in Fig. 1B. The reaction sequence starts with the reduction of HMG-CoA to a transient mevaldyl-CoA intermediate using the first NAD(P)H molecule; the intermediate is protonated and converted to mevaldehyde and CoA. The mevaldehyde intermediate is trapped in the active site and reduced to mevalonate by the next reduction step using the second NAD(P)H molecule [2]. Notably, in the course of the catalytic reactions, HMGR releases CoA and exchanges the first reaction product $NAD(P)^+$ with the second NAD(P)H without release of the mevaldehyde intermediate [10]. Despite the similar structures of the active site of class-I and -II HMGRs, class-I enzymes have a higher sensitivity to statins compared to class-II enzymes [11,12]. This discrepancy is due to the different organizations of the active site [13].

The catalytic mechanism of class-I and class-II HMGRs has been studied based on several crystal structures in complex with different combinations of substrates, intermediates and products [14,15]. Both types of HMGRs involve conformational rearrangements of the C-terminal region during the catalytic cycle. Class-II HMGR from *Pseudomonas mevalonii* contains a flexible C-terminal flap domain, which closes the active site when the ternary complexes are formed [15]. When only the HMG-CoA substrate is bound to class-II HMGR in *Streptococcus pneumoniae*, the C-terminal flap only partially closes [10]. The human class-I HMGR has a short C-terminal helix (called helix Lα11 in the large subdomain) instead of the C-terminal flap domain in class-II enzymes. When HMG-CoA or CoA substrates are bound, its C-terminal extension is partially fixed. Only when $NADP^+$, HMG and CoA substrates or more likely when $NADP^+$ and HMG-CoA substrates are simultaneously bound, the C-terminal helix Lα11 binds to the protein core and is stabilized [14]. In this configuration, the active site is closed, and HMG-CoA is completely covered by the Lα11 helix. This structural rearrangement suggests that the C-terminal flap domain in class-II enzymes and the

helix Lα11 in class-I enzymes have crucial functions to sequester the reaction intermediates (mevaldyl-CoA and mevaldehyde) and to perform catalysis. To elucidate the complete conformational rearrangement process in the catalytic cycle of class-I enzymes, the structures of the apoenzyme and its complex with only the NADPH substrate are required.

Here, we report the kinetic properties and crystal structure of the class-I HMGR from *Methanothermococcus thermolithotrophicus* (mHMGR), a thermophilic methanogenic archaeon. In the crystal structures of the mHMGR apoenzyme and its complex with NADPH, the C-terminal Lα11 helix connects with the Lα10 helix to form an elongated straight helix (Lα10-11) (nomenclature of helices is derived from human class-I HMGR), and the active site is completely open to the solvent. Based on this finding, we propose a refined picture of the conformational rearrangements of the C-terminal helix induced by binding of the substrates in class-I HMGRs.

Materials and methods

Chemicals and reagents

The HMG-CoA, isopropyl β-D-1-thiogalactopyranoside (IPTG), piperazine-N,N′-bis(2-ethanesulfonic acid) (PIPES), 2-(N-morpholino) ethanesulfonic acid (MES), dithiothreitol (DTT), simvastatin and all other buffers used in this work were purchased from Sigma-Aldrich, GmbH. NADPH was from Biomol, GmbH.

Culturing *Methanothermococcus thermolithotrophicus* and inhibition by simvastatin

Methanothermococcus thermolithotrophicus was grown at 65 °C in 150-mL bottles containing 10 mL of the growth medium described by Belay *et al.* [16] with an addition 1 μM $NaHSeO_3$, 25 mM PIPES and 25 mM 2-(N-morpholino)ethanesulfonic acid (MES) under the gas phase 20% CO_2/80% H_2 under +0.6 bar[17]. To reduce the medium, 2 mM $Na_2S{\cdot}9H_2O$ (final concentration) was added by 0.2-μm filter (Sartorius). Simvastatin was solubilized in dimethyl sulfoxide at a concentration of 25 mM and added to the media by a syringe at the indicated final concentration. The growth experiments were started by the addition of 0.4 mL of *M. thermolithotrophicus* preculture.

HMGR expression and purification

The mHMGR-encoding gene was cloned and expressed, and the His-tagged protein was purified using Ni-affinity chromatography as described previously [18]. In this work, mHMGR was further purified with a HiLoad™ 16/600 Superdex™ 200 pg (GE Healthcare, Freiburg, Germany) using 20 mM Tris-HCl pH 8.0 and 150 mM NaCl. Glycerol and DTT were added to an aliquot of the purified fraction at a final concentration of 20% v/v and 10 mM, respectively, and the fractions were stored at −20 °C before activity assays. Another aliquot was directly used for crystallization without freezing. The protein concentrations were determined spectrophotometrically ($\varepsilon_{280\ nm}$ = 23.8 $cm^{-1}{\cdot}mM^{-1}$).

HMGR enzyme activity assay

The mHMGR enzyme activity was measured at 60 °C by detecting NADPH consumption at 340 nm using a Carry-60 UV-Vis spectrophotometer (Agilent, Waldbronn, Germany) with 10 mm quartz cuvettes (Hellma, Mülheim, Germany). The assay mixture for k_{cat} and $K_{M,app}$ for HMG-CoA contained 500 mM potassium phosphate buffer pH 7.5, 20 mM KCl, 10 mM DTT, 300 μM NADPH, various amounts of HMG-CoA and 33 nM mHMGR. The reaction was started by the addition of the enzyme. The assay mixture for k_{cat} and $K_{M,app}$ for NADPH contained 500 mM potassium phosphate buffer pH 7.5, 20 mM KCl, 10 mM DTT, 200 μM HMG-CoA, various amounts of NADPH, and 33 nM mHMGR. One unit of enzyme is defined as the amount that catalyses the oxidation of 1 μmol of NADPH per min. All assays were started with addition of the enzyme. The assays to determine simvastatin inhibition contained 500 mM potassium phosphate buffer pH 7.5, 10 mM DTT, 300 μM NADPH, 50 μM HMG-CoA, 15 nM mHMGR and variable amounts of simvastatin.

Crystallization

The mHMGR was concentrated to 10 $mg{\cdot}mL^{-1}$ with an Amicon Ultra-4 Centrifugation filter (30 kDa cut-off) (Millipore, Darmstadt, Germany) centrifuged at 11 337 ***g*** for 5 min at 4 °C to remove any aggregates and dust. mHMGR was crystallized using the sitting drop vapour diffusion method at 18 °C. The 0.7 μL protein sample was spotted on a 96-well 2-drop MRC Crystallization Plate (Molecular Dimensions, Suffolk, UK), and 0.7 μL of reservoir solution was mixed. The best crystals were obtained after several months using a solution containing 40% v/v poly(ethylene glycol) 400, 100 mM Tris/HCl pH 8.5 and 200 mM Li_2SO_4. mHMGR was crystallized with 2 mM NADPH under the same conditions. The crystals in the apo form had a long rod shape. The crystals containing NADPH had a prism shape.

Data collection and refinement

The mHMGR crystals in the apo form and in complex with NADPH were directly flash-frozen in liquid nitrogen.

The diffraction experiments were performed at 100 K on the ID23-1 beamline at the European Synchrotron Radiation Facility (ESRF) equipped with a Pilatus 6M (Dectris) detector. The data were processed with XDS [19] and scaled with SCALA [20] from the CCP4 SUITE [20]. The apoenzyme structure was determined by molecular replacement with PHASER from the PHENIX package [21] by using the monomer of human HMGR in complex with the HMG and CoA substrates (PDB: 1DQ8) as a template. The structure of HMGR in complex with NADP was solved with PHASER by using the refined apo structure. The first model of the apoenzyme form was built with the BUCCANEER software [22], and the models were manually built with COOT [23] and refined with BUSTER (G. Bricogne *et al*. Cambridge, United Kingdom: Global Phasing Ltd., 2016) or PHENIX [21]. The final refinement cycles contained the hydrogens in riding position. The final models were validated by using MOLPROBITY [24]. Data collection, refinement statistics, and PDB codes for the deposited model are listed in Table 1. The hydrogens were omitted in the final deposited model. NADPH was modelled in all six monomers of the asymmetric unit, where the electron density is present at the adenine and pyrophosphate moieties and a part of the ribose. The figures were generated and rendered with PYMOL (Version 1.7, Schrödinger, LLC).

Bioinformatics analysis

The enzymatic parameters and fits were determined with GRAPHPAD PRISM 7 (San Diego, CA, USA). Sequence alignment was performed by the Clustal Omega server from EBI, and the output was illustrated by the ESPRIPT server [25]. The same sequence alignment was superimposed on the 3D structure using the CONSURF server [26].

Results

Kinetic properties of mHMGR

N-terminal His-tagged mHMGR was heterologously produced in *Escherichia coli* and purified using a His-Trap column followed by gel filtration (Fig. S1). The gel filtration profile of the purified enzyme was consistent with a homotetrameric assembly as previously reported for other class-I HMGRs [14] (Fig. S1B). mHMGR had kinetic parameters (k_{cat} = 15 ± 2 s^{-1}, V_{max} = 19 ± 2 U·mg^{-1}, $_{app}K_M$ for HMG-CoA = 13 ± 1 μM, $_{app}K_M$ for NADPH = 57 ± 8 μM) (Fig. S2) within the same order of magnitude as those previously reported for HMGR from Syrian hamster (k_{cat} = 31 s^{-1}, V_{max} = 37 U·mg^{-1}, $_{app}K_M$ for HMG-CoA = 4.3 μM) [27,28] and other archaea including *Sulfolobus solfataricus* (k_{cat} = 12 s^{-1}, V_{max} = 17 U·mg^{-1}, $_{app}K_M$ for HMG-CoA = 17 μM) [28] and *Haloferax volcanii* (k_{cat} = 23 s^{-1}, V_{max} = 34 U·mg^{-1}, $_{app}K_M$ for HMG-CoA = 60 μM) [28,29].

Table 1. X-ray analysis statistics.

	Apo mHMGR	mHMGR cocrystallized with NADPH
Data collection		
Wavelength (Å)	0.97662	0.97662
Space group	$P3_112$	$P4_12_12$
Resolution (Å)	42.61–2.40 (2.53–2.40)	25.00–2.90 (3.06–2.90)
Cell dimensions		
a, b, c (Å)	83.3, 83.3, 211.2	231.8, 231.8, 98.7
α, β, γ (°)	90, 90, 120	90, 90, 90
R_{merge}(%)[a]	8.9 (117.7)	9.5 (128.5)
R_{pim} (%)[a]	2.9 (37.5)	3.7 (49.1)
$CC_{1/2}$ (%)[a]	99.9 (63.4)	99.9 (42.7)
I/σ_I[a]	16.5 (2.1)	13.3 (1.6)
Completeness (%)[a]	99.7 (100.0)	99.8 (100.0)
Redundancy[a]	10.2 (10.8)	7.3 (7.7)
Number of unique reflections[a]	33 184 (4821)	59 867 (8592)
Refinement		
Resolution (Å)	42.61–2.40	25.00–2.90
Number of reflections	33 130	59 830
R_{work}/R_{free}[b] (%)	17.27/21.98	21.11/24.26
Number of atoms		
Protein	6050	17 794
Ligands/ions	69	279
Solvent	41	0
Mean B-value (Å^2)	68.2	113.0
Molprobity clash score, all atoms	2.98 (100th percentile)	1.66 (100th percentile)
Ramachandran plot		
Favoured regions (%)	97.33	96.23
Outlier regions (%)	0	1
rmsd bond lengths (Å)	0.007	0.003
rmsd bond angles (°)	0.843	0.653
PDB code	6HR7	6HR8

rmsd, root mean square deviation.
[a]Values relative to the highest resolution shell are within parentheses.
[b]R_{free} was calculated as the R_{work} for 5% of the reflections that were not included in the refinement.

As shown in Fig. S3A, simvastatin lactone (a statin inhibitor) strongly inhibited mHMGR ($_{app}K_i$ = 2.9 ± 0.8 nM) similar to the degree of statin inhibition on class-I HMGRs, such as human HMGR ($_{app}K_i$ = 11 nM for simvastatin) [30] and archaeal HMGRs including *S. solfataricus* HMGR ($_{app}K_i$ for Lovastatin = 5 nM) [31] and *H. volcanii* HMGR ($_{app}K_i$ for Lovastatin lactone = 15 μM and $_{app}K_i$ for Lovastatin free-acid 15 nM) [29]. We also tested the effect of simvastatin lactone on the growth of *M. thermolithotrophicus* (Fig. S3B). The growth rate

decreased by 50% in 10–20 nM simvastatin lactone. This concentration was within the range of $_{app}K_i$ of simvastatin lactone for the purified enzyme activity measurements in this work but was much lower than the lovastatin (a statin) concentration (4–10 μM) required for 50% inhibition of the methanogenic

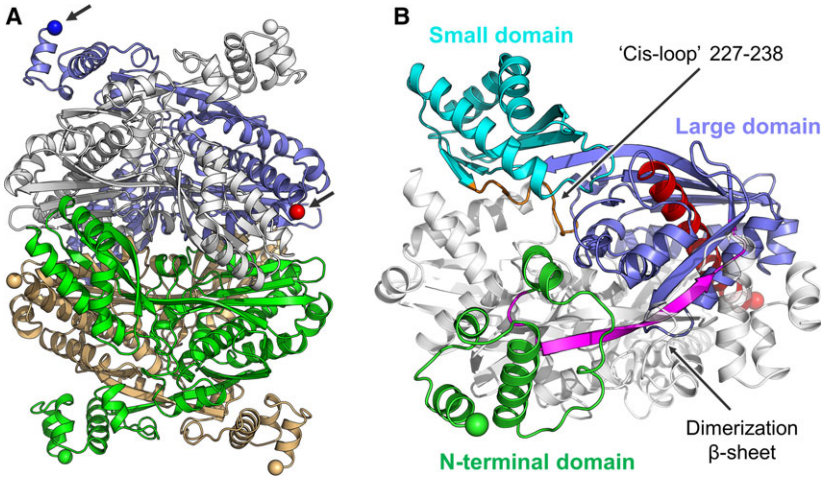

Fig. 2. Structural overview of mHMGR. (A) Each chain in the tetrameric structure is denoted with a different colour. The two black arrows point to the N- and C termini (Asn6 to His401) of one monomer, which are highlighted by blue and red balls, respectively. (B) Close-up view of the dimer functional unit, with one monomer shown in transparent white for clarity. N-terminal (1–65, in green), large (66–132 and 239–406, in blue) and small domains (133–226, in cyan), *cis*-loop (227–238, in orange), dimerization β-sheet (66–82, in pink) and C-terminal helix Lα10-11 (369–401, in red).

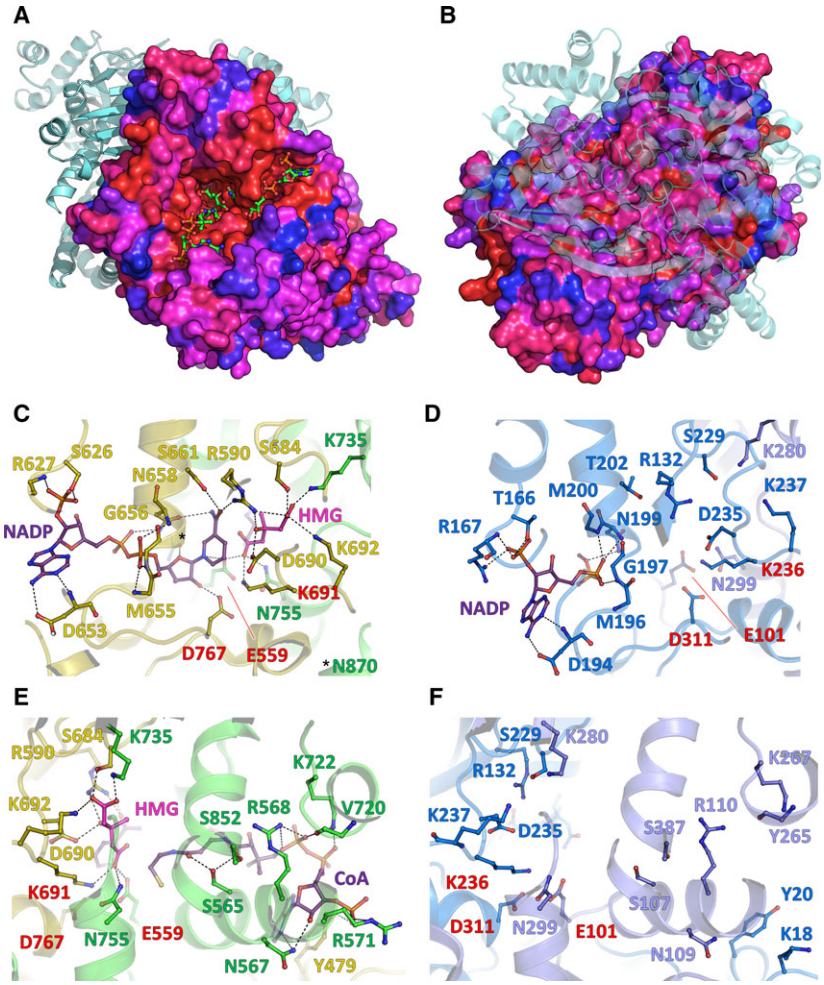

Fig. 3. Active site conservation between mHMGR and human HMGR. (A) One dimer of mHMGR is shown in the surface model with colour codes reflecting the sequence conservation from the alignment of Fig. S5 ranging from red (perfectly conserved) to blue (not conserved). The second dimer is shown as a transparent cyan in the figure. The ligands (NADPH, CoA-SH and HMG) are shown as green sticks based on the superposition with human HMGR (PDB 1DQA). (B) The same representation as in A turned by 180° along the *Y* axis. (C) Human HMGR (PDB: 1DQA) active site viewed from NADP, where the hydrogen-bonded residues with NADP (in purple) and HMG (in pink) are represented in balls and sticks. (D) The mHMGR NADPH-bound structure in the same view as in panel C. (E) Human HMGR (PDB: 1DQA) active site viewed from CoA (in purple). (F) The mHMGR NADPH-bound structure in the same view as in panel E.

archaea that inhabit rumen (i.e., *Methanobrevibacter*) [32,33].

Crystal structure of mHMGR apoenzyme

After extensive crystallization trials for mHMGR in the apoenzyme state, we obtained a trigonal crystalline form that diffracted to 2.4 Å. The crystal structure was solved using molecular replacement with the human HMGR as the template (Table 1). The methanogenic HMGR is a dimer of homodimers (Fig. 2A); its folding pattern was nearly identical to the catalytic domain of the human homologue, with a root mean square deviation of 0.719 Å for one monomer (with a superposition of 297 Cα from the PDB: 1DQA, Fig. S4) according to the high conservation of the protein sequence (7–401; 42% identity and 63% similarity) (Fig. S5). The monomers of HMGR contained an N-terminal (1–65), large (66–132 and 238–406) and small (133–226) domains and a *cis*-loop (227–237) (Figs 2B and S6).

The residues involved in oligomerization were less conserved than those surrounding the active site (Fig. 3A,B). The area involved in oligomerization of mHMGR had more hydrogen bonds and fewer salt bridges compared to human HMGR; there were a total of 224 hydrogen bonds in mHMGR compared to 179 in the human homologue and 18 salt bridges in mHMGR compared to 34 in the human homologue, as calculated from the PISA server (http://www.ebi.ac.uk/pdbe/pisa/). There was a notable structural difference between mHMGR and the human version in the C-terminal helix (369–401). In the apoenzyme structure of mHMGR, the C-terminal helix (Lα11) was connected to Lα10 to form an elongated helix (Lα10-11), which made the active site open for entrance of the substrates (Figs 4 and S7). The modelled Lα10 (369–394) and Lα11 (395–401) of the C-terminal helix of

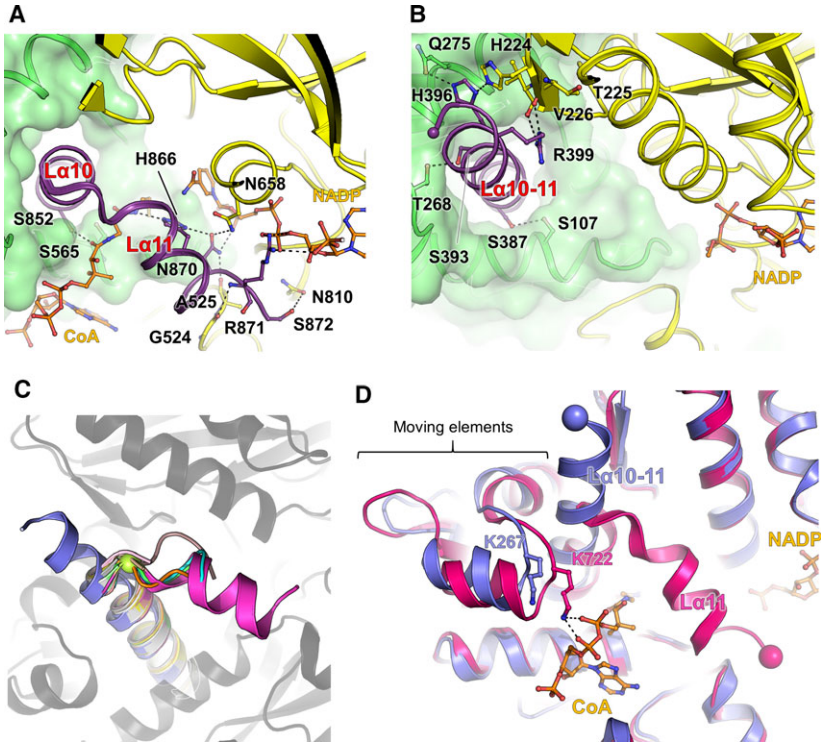

Fig. 4. Structural comparison of the C-terminal helix in mHMGR and the human enzyme. (A) Hydrophilic contacts in Lα11 of human HMGR in complex with HMG, CoA and NADP (PDB: 1DQA, HMG has been omitted for clarity). (B) The same view as A for mHMGR complexed with NADPH. The sphere at the end of the C-terminus shows the position of the His401. (C) Superposition of the structures of human HMGR: the ternary complex with HMG, CoA and NADP (1DAQ, in pink); the complex with HMG-CoA (1DQ9, in cyan); the complex with HMG and CoA (1DQ8, in green) and the other structures in complex with statins (in different colours). mHMGR is superposed and shown in a purple colour. Only mHMGR secondary structures are shown as black cartoon to clarify the figure. The green ball indicates the hinge region between Lα10 and Lα11. (D) Superposition of mHMGR (in purple) and human HMGR (in pink) represented as cartoons. The human structural elements that deviate from mHMGR are highlighted by a brace, which correspond to the β-sheet-helix-loop-helix (251–277) and the β-hairpin (323–340) in mHMGR.

mHMGR are highly similar to those of human HMGR (Lα10: 50% identity and 70% similarity and Lα11: 40% identity and 60% similarity) (Fig. S5). The C-terminal helix was connected to the β-sheet-helix-loop-helix (251–277) and the β-hairpin (323–340), which shifted of ~ 3 Å compared to the human HMGR (Fig. 4D).

Crystal structure of mHMGR in complex with NADPH

We cocrystallized mHMGR with NADPH as a tetragonal crystalline form that diffracted to 2.9 Å (Table 1). The asymmetric unit contained one and a half tetramers, which superposed well to the apo-crystal structure of mHMGR with a root mean square deviation of 0.245 Å for 750 superposed Cα. A clear electron density was detected for the adenine mononucleotide moiety of NADPH for all six monomers composing the asymmetric unit (Figs 5A,C). The 2′-phosphate on the ribose moiety was fixed *via* hydrogen bonds between His168, Thr166 and Arg167, which determined the specificity for NADPH. The adenine ring was stacked between His168 and Val346 and stabilized *via* two hydrogen bonds from Asp194 in the same fashion than the human homologue (Fig. 5B). The electron density disappeared after the second phosphate group of the pyrophosphate moiety, which indicates a high flexibility of the nicotinamide mononucleotide in this form. All six monomers in the asymmetric unit had the same conformation of the C-terminal helix as observed in the mHMGR apoenzyme structure, which suggests that NADPH binding does not induce the closed conformation of the active site.

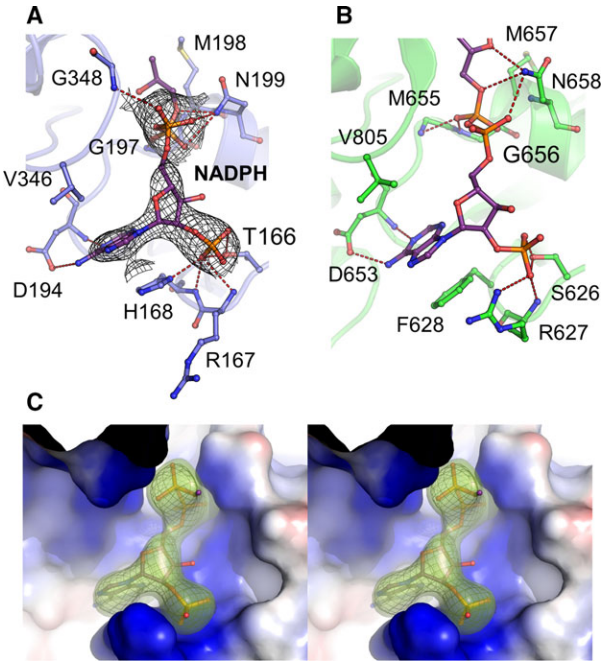

Fig. 5. The NADPH-binding site. (A) Close view of the NADPH-binding site in mHMGR where NADPH and the residues in proximity to NADPH are shown as balls and sticks. Hydrogen bonds and salt bridges are indicated as red dashed lines, and the electron density corresponding to the $2F_o-F_c$ is contoured at 1.3 σ. (B) Same view and representation of panel A with the superposed human HMGR (PDB code: 1DQA). (C) Stereo view of NAPDH bound to mHMGR (shown as balls and sticks) and its omit map contoured at 1.3 σ in grey mesh. In addition, the difference map F_o-F_c contoured at 3.0 σ is represented as a transparent green surface. The electrostatic profile of mHMGR is shown as a surface and the negative to positive potential is coloured from red to blue respectively.

Active site structure

The active site residues of mHMGR and human HMGR were structurally fully conserved (Fig. 3). The *cis*-loop (residues 227–238 in mHMGR, Figs 2B and S6) adopts the same configuration as in the human HMGR structure. We identified the catalytic residues based on the human homologue structure. Lys691 in the human enzyme is proposed to stabilize the negatively charged intermediate mevaldyl-CoA (Fig. 1B) [14] and is perfectly superposable with Lys236 in mHMGR (Fig. 3). The most probable proton donor for the mevaldehyde intermediate in mHMGR was Glu101, which should be in a protonated state by the proximity of Asp311 (3.1 Å). These residues were also superposable between mHMGR and human HMGR (Glu559 and Asp767). We compared the mHMGR apoenzyme structure with the structure of the human HMGR in complex with a statin (simvastatin) (Fig. S8). The simvastatin-binding site structure was almost identical to that of mHMGR. This agrees with the high affinity of statin inhibitors for mHMGR.

Discussion

In this study, we presented the first crystal structure of a class-I HMGR from an archaeon. The amino acid residues involved in substrate recognition and activation are almost identical to those of human HMGR, which agrees with the similar kinetic parameters and inhibition constants for simvastatin lactone. In the structure of human HMGR complexed with HMG, CoA and $NADP^+$ substrates, the active site is locked and encapsulated by the C-terminal helix (Lα11), which could act as the flap domain in class-II HMGR to close the active site.

The structural movements orchestrating the substrate binding and catalysis in class-II HMGR have been characterized through different crystal structures [9,10,15]. These conformational changes involve mainly the C-terminal domain, which flips and coordinates the binding/releasing of the substrates during the reaction. The structures from HMGR of *Streptococcus pneumoniae* shows that NADPH binding is not enough to promote the flipping of the C-terminal domain (open state) and it seems that HMG-CoA drives the first conformational change into a 'partially closed' state [10]. When both substrates bind, the C-terminal domain completely closes the active site [14]. In class-I HMGR, this C-terminal domain is replaced by the C-terminal helix Lα11 which is elongated (Lα10-11) in mHMGR and kinked in the human enzyme bound to its substrates. In this elongated conformation, the active site is fully open to bulk solvent. Our crystal structure of mHMGR in complex with NADPH indicated that NADPH binding does not trigger the conformational rearrangement of the C-terminal helix as observed for *S. pneumoniae* class-II HMGR with the C-terminal domain.

In human HMGR, His866 at the start of Lα11 is located at a hydrogen bond distance from the thiol of the CoA molecule; His866 is proposed to be the proton donor for the thioanion [14,34]. The equivalent His401 in mHMGR is located at the C-terminal end of the elongated helix (Lα10-11) and is too far away to protonate the thioanion of CoA in this open conformation (Figs 4 and 6). However, His401 is conserved in all archaeal HMGRs (Fig. S5), and mutation of this histidine to glutamine in the archaeal HMGR from *H. volcanii* decreases the activity by 100-

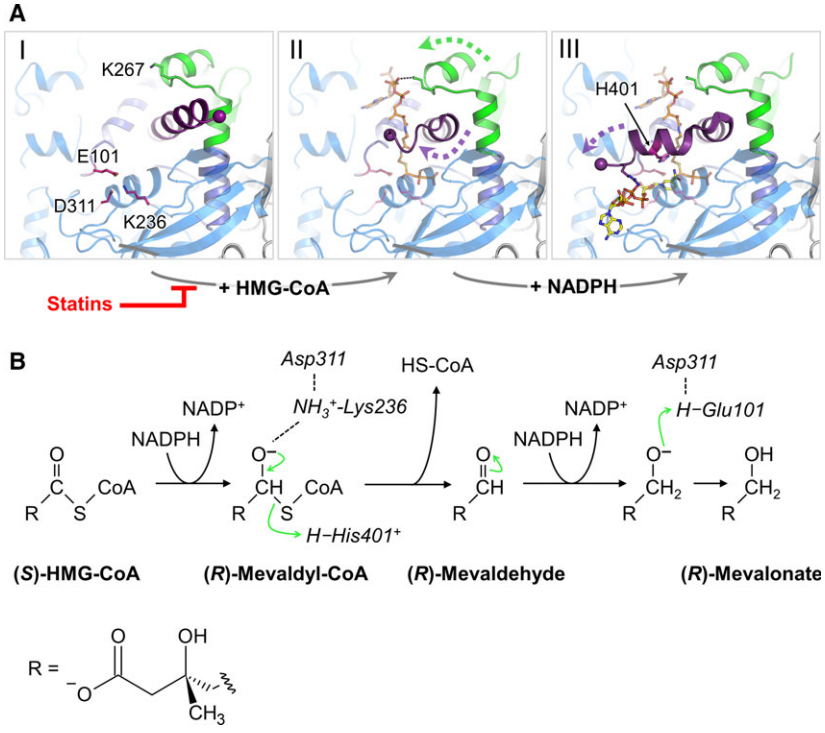

Fig. 6. The conformational rearrangement upon substrates binding and the catalytic reactions. (A) We proposed at least three-step rearrangements during catalysis: (I) the open apoenzyme form, (II) first substrate bound, partially closed form and (III) the ternary complex, close form. Other intermediate states might exist as seen in class-II HMGR [9]. In the reaction sequence, either HMG-CoA or NADPH may bind first; only if NADPH binds first, the La10-11 helix remains elongated. To show the formation of step (II), the first substrate bound is modelled as HMG-CoA (see Discussion). Since the structure of mHMGR in complex with HMG-CoA or HMG-CoA and NADPH are not available, the backbone of mHMGR (shown in blue) has been kept in panel II and III but the added substrates and conformational movements are modelled based on human HMGR structures bound with HMG-CoA (PDB: 1DQ9) and human HMGR bound with $NADP^+$, CoA and HMG (PDB: 1DQA) respectively. The green dashed arrow illustrates the movement of the β-sheet-helix-loop-helix 251–277 and β-hairpin 323–340, and the purple arrow shows the movement of the Lα11 helix. Catalytic residues are highlighted in pink, HMG-CoA (orange) and NADPH (yellow) are shown as balls and sticks. The C-terminal helix is coloured in purple and the β-sheet-helix-loop-helix 251–277 and β-hairpin 323–340 involved in structural rearrangements are shown in green. (B) The reactions and roles of catalytic residues from mHMGR based on the catalytic functions of residues of human HMGR.

fold. This result supports the hypothesis that, in the closed conformation, Lα11 in mHMGR is kinked, and His401 hydrogen bonds with the thiol of CoA [35].

The crystal structures that we presented of archaeal class-I HMGR (mHMGR) fully complement the structures of class-I human HMGR in the catalytic cycle that were lacking. Based on the high sequence identity between human and archaeal HMGR and the previous observation that His401 is essential in *H. volcanii* HMGR, we propose a fairly complete picture of the structural rearrangements of class-I HMGR involved in catalysis. (a) In the apoenzyme structure, the C-terminal helix (Lα10-11) is straight and this leads to a fully open active site. (b) Binding of HMG-CoA repositions the β-sheet-helix-loop-helix (251–277) and the β-hairpin (323–340) (Fig. 4D) and kinks the Lα11 helix, while the C terminus containing catalytic His401 remains flexible. (c) Additional binding of NADPH induces conformational changes in the C-terminal helix to close the active site (Fig. 6A). After these conformational rearrangements, the C-terminal helix fully wraps around the HMG moiety of HMG-CoA and fixes the nicotinamide nucleotide moiety of NADPH. However, our work does not exclude the possibility of another sequence of substrate binding; NADPH first and then HMG-CoA. In this case, the reaction sequence does not proceed *via* form II because the NADPH binding alone does not induce the structural change (Figs 5A and 6A). The conserved Arg871 in human HMGR (Fig. S5) contributes to NADPH binding, whereas the corresponding Arg406 of mHMGR is disordered in the crystal structure of even in the NADPH-binding form, probably because Arg406 could not interact with NADPH in the elongated structure. Upon binding of both HMG-CoA and NADPH to the active site, the C-terminal residue Arg406 might act as a hook to completely close the active site. Once locked, HMG-CoA is reduced to mevaldyl-CoA with NADPH. In the closed conformation, CoA and $NADP^+$ are dissociated from the active site, but mevaldehyde is still tightly bound. After reduction of mevaldehyde, disengagement of the second $NADP^+$ and mevalonate from the enzyme causes the Lα11 helix to return to its original straight conformation and expose the active site to the solvent.

In eukaryotes, HMGR is tightly controlled *via* serine phosphorylation. Phosphorylation of Ser871 in the Syrian hamster HMGR dramatically decreases enzyme activity [36,37]. Based on the apoenzyme structure of mHMGR, we hypothesize that phosphorylated Ser871 does not interfere with the catalytic reaction but hinders conformational rearrangements by stabilizing the straight conformation of Lα10-11 *via* salt bridges with the protein surface.

Statins are competitive inhibitors of HMG-CoA, and part of their chemical structure is analogous to HMG. Istvan and Deisenhofer argued that binding of bulky statins exploits the flexibility of the C-terminal Lα11 helix to be bound in the open conformation. The archaeal structure presented here indicates that class-I HMGR is fully open in the apoenzyme form, in which statins could easily bind and inhibit the enzyme. The structural conservation between human and archaeal HMGR explains the effects of statins' inhibitors against archaeal mevalonate biosynthesis *in vivo* and *in vitro*.

Acknowledgements

We thank Dr. S. Engilberge and Dr. E. Girard (IBS, Grenoble) for providing us synchrotron time for the X-ray diffraction experiments. We thank the staff of the ID23-1 beamline at ESRF for their advice during data collection. This work was supported by a grant from the Max Planck Society to SS and TJE and a grant from the LOEWE Program MEGASYN for TJE.

Author contributions

TW and BV conceived the study, designed the experiments and crystallized the enzyme. BV cloned, expressed, purified and assayed the enzyme. TW performed the crystallographic studies, refinement and deposition of the structures. TW, BV, TJE and SS analysed data and wrote the manuscript.

References

1 Miziorko HM (2011) Enzymes of the mevalonate pathway of isoprenoid biosynthesis. *Arch Biochem Biophys* **505**, 131–143.
2 Istvan ES and Deisenhofer J (2000) The structure of the catalytic portion of human HMG-CoA reductase. *Biochim Biophys Acta* **1529**, 9–18.
3 Endo A (2010) A historical perspective on the discovery of statins. *Proc Jpn Acad Ser B* **86**, 484–493.
4 Haines BE, Wiest O and Stauffacher CV (2013) The increasingly complex mechanism of HMG-CoA reductase. *Acc Chem Res* **46**, 2416–2426.
5 Istvan ES (2001) Bacterial and mammalian HMG-CoA reductases: related enzymes with distinct architectures. *Curr Opin Struct Biol* **11**, 746–751.
6 Friesen JA and Rodwell VW (2004) The 3-hydroxy-3-methylglutaryl coenzyme-A (HMG-CoA) reductases. *Genome Biol* **5**, 248.

7 Johnson BM and DeBose-Boyd RA (2017) Underlying mechanisms for sterol-induced ubiquitination and ER-associated degradation of HMG CoA reductase. *Semin Cell Dev Biol* **81**, 121–128.

8 Kim DY, Stauffacher CV and Rodwell VW (2000) Dual coenzyme specificity of *Archaeoglobus fulgidus* HMG-CoA reductase. *Protein Sci* **9**, 1226–1234.

9 Ragwan ER, Arai E and Kung Y (2018) New crystallographic snapshots of large domain movements in bacterial 3-hydroxy-3-methylglutaryl coenzyme A reductase. *Biochemistry* **57**, 5715–5725.

10 Miller BR and Kung Y (2018) Structural features and domain movements controlling substrate binding and cofactor specificity in class II HMG-CoA reductase. *Biochemistry* **57**, 654–662.

11 Wilding EI, Kim DY, Bryant AP, Gwynn MN, Lunsford RD, McDevitt D, Myers JE Jr, Rosenberg M, Sylvester D, Stauffacher CV *et al*. (2000) Essentiality, expression, and characterization of the class II 3-hydroxy-3-methylglutaryl coenzyme A reductase of *Staphylococcus aureus*. *J Bacteriol* **182**, 5147–5152.

12 Tabernero L, Rodwell VW and Stauffacher CV (2003) Crystal structure of a statin bound to a class II hydroxymethylglutaryl-CoA reductase. *J Biol Chem* **278**, 19933–19938.

13 Istvan ES and Deisenhofer J (2001) Structural mechanism for statin inhibition of HMG-CoA reductase. *Science* **292**, 1160–1164.

14 Istvan ES, Palnitkar M, Buchanan SK and Deisenhofer J (2000) Crystal structure of the catalytic portion of human HMG-CoA reductase: insights into regulation of activity and catalysis. *EMBO J* **19**, 819–830.

15 Tabernero L, Bochar DA, Rodwell VW and Stauffacher CV (1999) Substrate-induced closure of the flap domain in the ternary complex structures provides insights into the mechanism of catalysis by 3-hydroxy-3-methylglutaryl-CoA reductase. *Proc Natl Acad Sci USA* **96**, 7167–7171.

16 Belay N, Sparling R and Daniels L (1986) Relationship of formate to growth and methanogenesis by *Methanococcus thermolithotrophicus*. *Appl Environ Microbiol* **52**, 1080–1085.

17 Wagner T, Koch J, Ermler U and Shima S (2017) Methanogenic heterodisulfide reductase (HdrABC-MvhAGD) uses two noncubane [4Fe-4S] clusters for reduction. *Science* **357**, 699–703.

18 Vögeli B, Engilberge S, Girard E, Riobé F, Maury O, Erb TJ, Shima S and Wagner T (2018) Archaeal acetoacetyl-CoA thiolase/HMG-CoA synthase complex channels the intermediate via a fused CoA-binding site. *Proc Natl Acad Sci USA* **115**, 3380–3385.

19 Kabsch W (2010) XDS. *Acta Crystallogr D* **66**, 125–132.

20 Winn MD, Ballard CC, Cowtan KD, Dodson EJ, Emsley P, Evans PR, Keegan RM, Krissinel EB, Leslie AG, McCoy A *et al*. (2011) Overview of the CCP4 suite and current developments. *Acta Crystallogr D* **67**, 235–242.

21 Adams PD, Afonine PV, Bunkóczi G, Chen VB, Davis IW, Echols N, Headd JJ, Hung LW, Kapral GJ, Grosse-Kunstleve RW *et al*. (2010) *PHENIX*: a comprehensive Python-based system for macromolecular structure solution. *Acta Crystallogr D* **66**, 213–221.

22 Cowtan K (2006) The *Buccaneer* software for automated model building. 1. Tracing protein chains. *Acta Crystallogr D* **62**, 1002–1011.

23 Emsley P, Lohkamp B, Scott WG and Cowtan K (2010) Features and development of *Coot*. *Acta Crystallogr D* **66**, 486–501.

24 Chen VB, Arendall WB 3rd, Headd JJ, Keedy DA, Immormino RM, Kapral GJ, Murray LW, Richardson JS and Richardson DC (2010) *MolProbity*: all-atom structure validation for macromolecular crystallography. *Acta Crystallogr D* **66**, 12–21.

25 Robert X and Gouet P (2014) Deciphering key features in protein structures with the new ENDscript server. *Nucleic Acids Res* **42**, W320–W324.

26 Ashkenazy H, Abadi S, Martz E, Chay O, Mayrose I, Pupko T and Ben-Tal N (2016) ConSurf 2016: an improved methodology to estimate and visualize evolutionary conservation in macromolecules. *Nucleic Acids Res* **44**, W344–W350.

27 Frimpong K and Rodwell VW (1994) The active site of hamster 3-hydroxy-3-methylglutaryl-CoA reductase resides at the subunit interface and incorporates catalytically essential acidic residues from separate polypeptides. *J Biol Chem* **269**, 1217–1221.

28 Bochar DA, Brown JR, Doolittle WF, Klenk HP, Lam W, Schenk ME, Stauffacher CV and Rodwell VW (1997) 3-hydroxy-3-methylglutaryl coenzyme A reductase of *Sulfolobus solfataricus*: DNA sequence, phylogeny, expression in Escherichia coli of the *hmgA* gene, and purification and kinetic characterization of the gene product. *J Bacteriol* **179**, 3632–3638.

29 Bischoff KM and Rodwell VW (1996) 3-hydroxy-3-methylglutaryl-coenzyme a reductase from *Haloferax volcanii*: Purification, characterization, and expression in *Escherichia coli*. *J Bacteriol* **178**, 19–23.

30 Holdgate GA, Ward WH and McTaggart F (2003) Molecular mechanism for inhibition of 3-hydroxy-3-methylglutaryl CoA (HMG-CoA) reductase by rosuvastatin. *Biochem Soc Trans* **31**, 528–531.

31 Kim DY, Bochar DA, Stauffacher CV and Rodwell VW (1999) Expression and characterization of the HMG-CoA reductase of the thermophilic archaeon

Sulfolobus solfataricus. *Protein Expres Purif* **17**, 435–442.
32 Gottlieb K, Wacher V, Sliman J and Pimentel M (2016) Review article: inhibition of methanogenic archaea by statins as a targeted management strategy for constipation and related disorders. *Aliment Pharmacol Ther* **43**, 197–212.
33 Miller TL and Wolin MJ (2001) Inhibition of growth of methane-producing bacteria of the ruminant forestomach by hydroxymethylglutary l-SCoA reductase inhibitors. *J Dairy Sci* **84**, 1445–1448.
34 Frimpong K and Rodwell VW (1994) Catalysis by Syrian hamster 3-hydroxy-3-methylglutaryl-coenzyme A reductase. Proposed roles of histidine 865, glutamate 558, and aspartate 766. *J Biol Chem* **269**, 11478–11483.
35 Bischoff KM and Rodwell VW (1997) 3-Hydroxy-3-methylglutaryl-coenzyme A reductase of *Haloferax volcanii:* Role of histidine 398 and attenuation of activity by introduction of negative charge at position 404. *Protein Sci* **6**, 156–161.
36 Omkumar RV, Darnay BG and Rodwell VW (1994) Modulation of Syrian hamster 3-hydroxy-3-methylglutaryl-CoA reductase activity by phosphorylation. Role of serine 871. *J Biol Chem* **269**, 6810–6814.
37 Omkumar RV and Rodwell VW (1994) Phosphorylation of Ser^{871} impairs the function of His^{865} of Syrian hamster 3-hydroxy-3-methylglutaryl-CoA reductase. *J Biol Chem* **269**, 16862–16866.

Supporting information

Additional supporting information may be found online in the Supporting Information section at the end of the article.

Fig. S1. Protein purity and gel filtration profile of the methanogenic mHMGR.

Fig. S2. Kinetic parameters of mHMGR.

Fig. S3. Simvastatin lactone inhibition on mHMGR activity and growth of *M. thermolithotrophicus*.

Fig. S4. Superposition of mHMGR and human HMGR.

Fig. S5. Sequence conservation between archaeal and human HMGR (generated by the Espript server).

Fig. S6. Stereo view of the *cis*-peptide bond between Cys233 and Val234.

Fig. S7. Stereo view of the electron density for the C-terminal helix of apo mHMGR.

Fig. S8. Stereo view of the superposition of the mHMGR apoenzyme with human HMGR in complex with simvastatin.